

# Non-perturbative high-harmonic generation in the three-dimensional Dirac semimetal $\text{Cd}_3\text{As}_2$

Sergey Kovalev,<sup>1,7</sup> Renato M. A. Dantas,<sup>2,7</sup> Semyon Germanskiy,<sup>3</sup> Jan-Christoph Deinert,<sup>1</sup> Bertram Green,<sup>1</sup> Igor Ilyakov,<sup>1</sup> Nilesh Awari,<sup>1</sup> Min Chen,<sup>1</sup> Mohammed Bawatna,<sup>1</sup> Jiwei Ling,<sup>4,5</sup> Faxian Xiu,<sup>4,5</sup> Paul H. M. van Loosdrecht,<sup>3</sup> Piotr Surówka,<sup>2</sup> Takashi Oka,<sup>2,6\*</sup> and Zhe Wang<sup>1,3\*</sup>

1. Helmholtz-Zentrum Dresden-Rossendorf, Dresden, Germany
2. Max Planck Institute for the Physics of Complex Systems, Dresden, Germany
3. Institute of Physics II, University of Cologne, Cologne, Germany
4. State Key Laboratory of Surface Physics and Department of Physics, Fudan University, Shanghai, China
5. Collaborative Innovation Center of Advanced Microstructures, Nanjing, China
6. Max Planck Institute for Chemical Physics of Solids, Dresden, Germany
7. These authors contributed equally to the work.

\*Corresponding authors: oka@pks.mpg.de (T.O.) zhewang@ph2.uni-koeln.de (Z.W.)

**Harmonic generation is a general characteristic of driven nonlinear systems, and serves as an efficient tool for investigating the fundamental principles that govern the ultrafast nonlinear dynamics. In atomic gases<sup>1</sup>, high-harmonic radiation is produced via a three-step process of ionization, acceleration, and recollision by strong-field infrared laser. This mechanism has been intensively investigated in the extreme ultraviolet and soft X-ray regions<sup>2,3</sup>, forming the basis of attosecond research<sup>1</sup>. In solid-state materials, which are characterized by crystalline symmetry and strong interactions, yielding of harmonics has just recently been reported<sup>4,5,6,7,8,9,10,11,12,13,14,15,16,17,18,19</sup>. The observed high-harmonic generation was interpreted with fundamentally different mechanisms<sup>14,15,16,17,18,19,20,21,22,23</sup>, such as interband tunneling combined with dynamical Bloch oscillations<sup>4,5,6,7,8,9,10,11,12,14,20,22</sup>, intraband thermodynamics<sup>18</sup> and nonlinear dynamics<sup>23</sup>, and many-body electronic interactions<sup>15,16,17,18,21</sup>. Here, in a distinctly different context of three-dimensional Dirac semimetal, we report on experimental observation of high-harmonic generation up to the seventh order driven by strong-field terahertz pulses. The observed non-perturbative high-harmonic generation is interpreted as a generic feature of terahertz-field driven nonlinear intraband kinetics of Dirac fermions. We anticipate that our results will trigger great interest in detection, manipulation, and coherent control of the nonlinear response in the vast family of three-dimensional Dirac and Weyl materials.**

High-harmonic generation (HHG) in two-dimensional Dirac semimetals (single-layer graphene<sup>11,19,24</sup> and 45-layer graphene<sup>12</sup>) has been reported very recently for pump pulses both in the terahertz ( $10^{12}$  Hz, 1 THz  $\sim$  4 meV)<sup>12,19</sup> and mid- or near-infrared (0.2 – 0.8 eV) ranges<sup>11,24</sup>. Although previous theoretical investigations pointed out that the peculiar linear energy-momentum dispersion relation (Dirac cone) should be essential for HHG in graphene (see e.g. Ref.<sup>25,26,27</sup>), the strong dependence on pump laser frequencies observed in the experiments favors different mechanisms. For the mid- or

near-infrared HHG, the interband transitions (combined with Bloch oscillations) play the major role, while the linear dispersion relation is not a prerequisite<sup>11</sup>. A similar mechanism involving interband transitions can also be applied to THz HHG in lightly-doped multi-layer graphene, whereas exact shape of the carrier distribution was found to only play a minor role<sup>12</sup>. In contrast, for heavily electron-doped graphene, intraband processes become important and HHG was ascribed to THz-field heated hot-electrons while assuming the electron subsystem thermalized quasi-instantaneously<sup>19</sup>.

One may expect to observe THz HHG universally in the Dirac materials also of higher dimension, e.g. three-dimensional (3D) Dirac or Weyl semimetals. However, THz HHG so far has not been reported for this class of materials, and the mechanism for observing THz HHG in a 3D Dirac material remains elusive. Here we report on time-resolved detection of non-perturbative THz HHG in the 3D Dirac semimetal  $\text{Cd}_3\text{As}_2$ , and a real-time theoretical analysis of the THz-field driven kinetics of the Dirac fermions that is directly linked to the linear dispersion relation. Our results show that the THz-field driven nonlinear kinetics of the Dirac electrons is the mechanism responsible for the efficient generation of high-harmonic radiation, as well as for its non-perturbative fluence dependence in  $\text{Cd}_3\text{As}_2$ .

As being both theoretically predicted and experimentally confirmed<sup>28,29,30,31,32,33</sup>,  $\text{Cd}_3\text{As}_2$  is a well-established room-temperature 3D Dirac semimetal with Fermi velocity about  $10^5$ - $10^6$  m/s. Very compelling topological properties such as topological surface states and 3D quantum Hall effects have been realized in this system<sup>34,35,36,37,38</sup>. In high-quality  $\text{Cd}_3\text{As}_2$  thin films prepared by molecular beam epitaxy (see Methods)<sup>39</sup>, we observe HHG unprecedentedly up to the seventh order in the non-perturbative regime. THz harmonic radiations were recorded with femtosecond resolution at room temperature (see Methods). Figure 1a displays the detected electric field as a function of time delay for the third

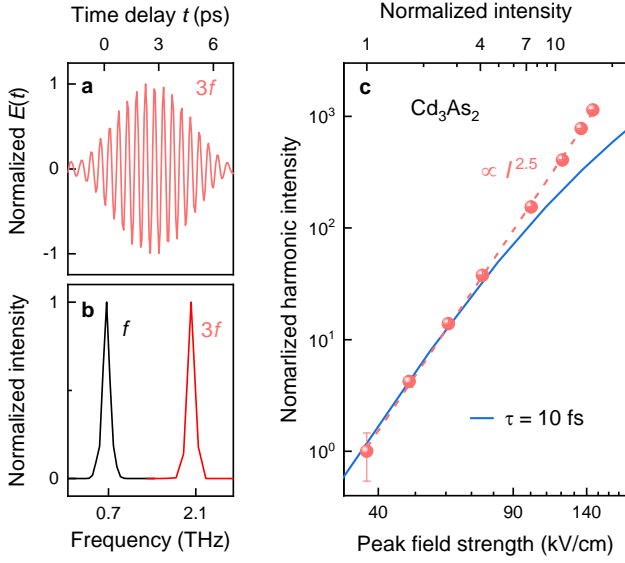


**Fig. 1 | Third harmonic generation in  $\text{Cd}_3\text{As}_2$ .** **a**, Time-resolved third-harmonic radiation characterized by its time-dependent electric field  $E(t)$  recorded at room temperature. **b**, Normalized power spectra of the harmonic radiation  $3f = 2.01$  THz, and the excitation pulse  $f = 0.67$  THz. **c**, Dependence of the third-harmonic radiation intensity on the pump intensity (symbols) follows  $I_{3f} \propto I_f^{2.5}$  (dashed line). Fit of the theoretical results is shown for the relaxation time  $\tau = 10$  fs (solid line).

harmonic radiation, induced by a multi-cycle pump pulse (Fig. 2a) with a peak field of 144 kV/cm characterized by its central frequency of  $f = 0.67$  THz (Fig. 1b). The power spectrum of the harmonic radiation is obtained by Fourier transformation of the time-domain signals, which exhibits a sharp peak at  $3f = 2.01$  THz (Fig. 1b). To further characterize the third harmonic generation, we measured the time-resolved signals for different pump-pulse intensities. As summarized in Fig. 1c, the fluence dependence of the third harmonic radiations remarkably does not follow the cubic law, but exhibits a power-law dependence as  $I_{3f} \propto I_f^{2.5}$  on the pump-pulse intensity  $I_f$ , which reveals a non-perturbative nonlinear response.

To understand the non-perturbative harmonic generation, we performed real-time theoretical analysis of the THz driven kinetics of the 3D Dirac electrons. For the electron-doped system, interband electronic excitations are Pauli-blocked for the THz pulses, thus we focus on the intraband kinetics of the nonequilibrium state by adopting a statistical approach of the Boltzmann transport theory. The initial state of thermodynamic equilibrium is defined by the room-temperature Fermi-Dirac distribution  $f_0[\epsilon(\mathbf{p})] = \left[ 1 + e^{\frac{\epsilon(\mathbf{p}) - \epsilon_F}{k_B T}} \right]^{-1}$  for the 3D Dirac electrons obeying the linear dispersion relation  $\epsilon(\mathbf{p}) = v_F |\mathbf{p}|$ , with  $\mathbf{p}$  and  $v_F$  denoting momentum and Fermi velocity, respectively,  $\epsilon_F$  for Fermi energy,  $k_B$  the Boltzmann constant, and  $T$  for temperature. In

presence of the THz pulse, the driven transient state is characterized by distribution function  $f(t, \mathbf{p})$ , the time-dependent evolution of which is governed by the Boltzmann equation<sup>40,41</sup>

$$\left( \frac{\partial}{\partial t} + \frac{1}{\tau} \right) f(t, \mathbf{p}) - e \mathbf{E}(t) \cdot \nabla_{\mathbf{p}} f(t, \mathbf{p}) = \frac{f_0(\mathbf{p})}{\tau}$$

Where the linear dispersion relation has been implemented,  $e$  and  $\mathbf{E}(t)$  denote the electron charge and the THz electric field, respectively, and  $\tau$  is the characteristic relaxation time for intraband processes (see Methods). We note that  $\tau$  is the only phenomenological parameter, and the analysis is performed without further assumptions. In particular, we do not presume that the electron subsystem thermalizes quasi-instantaneously or a Fermi-Dirac distribution should be obeyed by the transient states. In contrast, by solving the Boltzmann equation, we obtain the real-time distribution of the transient state. By comparing it with equilibrium-state Fermi-Dirac distribution, we can claim whether the corresponding transient state is nearly thermalized or far from thermodynamic equilibrium. Furthermore, we can derive the time-dependent current density, hence the THz field-induced harmonic radiations, the fluence dependence of which can be compared to the experimental observations.

For the experimentally implemented THz pump pulses (see Fig. 2a for the waveform) with a typical electric-field peak strength of 110 kV/cm, the obtained current density (Fig. 2b) and transient-state distribution functions are illustrated in Figs. 2c-2f, corresponding to the representative time delays (red symbols) marked in Fig. 2a and Fig. 2b, for the experimental values of Fermi energy  $\epsilon_F = 118$  meV and Fermi velocity  $v_F = 7.8 \times 10^5$  m/s as estimated from Shubnikov-de Haas oscillations<sup>39</sup>, and the relaxation time  $\tau = 10$  fs. The electric field of the linearly-polarized pump pulse is set along the  $p_z$  direction.

The microscopic origin of HHG resides in the nonlinear kinetics of the electron distribution (see Fig. 2d-2f) combined with the linear energy-momentum dispersion relation. Before the pump pulse arrives, the electrons in the upper band are in thermodynamic equilibrium, and fills the Dirac-cone up to around the Fermi energy according to the Fermi-Dirac distribution (Fig. 2c). When the pump pulse is present, the electrons are not only accelerated by the THz electric fields, but at the same time also scattered. Although the latter process is dissipative, the former one can very efficiently accumulate energy into the electron subsystem, leading to a stretched and shifted distribution along the field. In particular, at the peak field (symbol point 2 marked in Fig. 2a), the distribution is most strongly stretched and shifted in the field direction (Fig. 2d) resulting in the maximum current density and a peculiar flat-peak-like feature (Fig. 2b), thereby leading to very efficient HHG. In clear contrast to the Fermi-Dirac distribution of thermodynamic equilibrium states that is spherically symmetric for the 3D Dirac semimetal (manifested

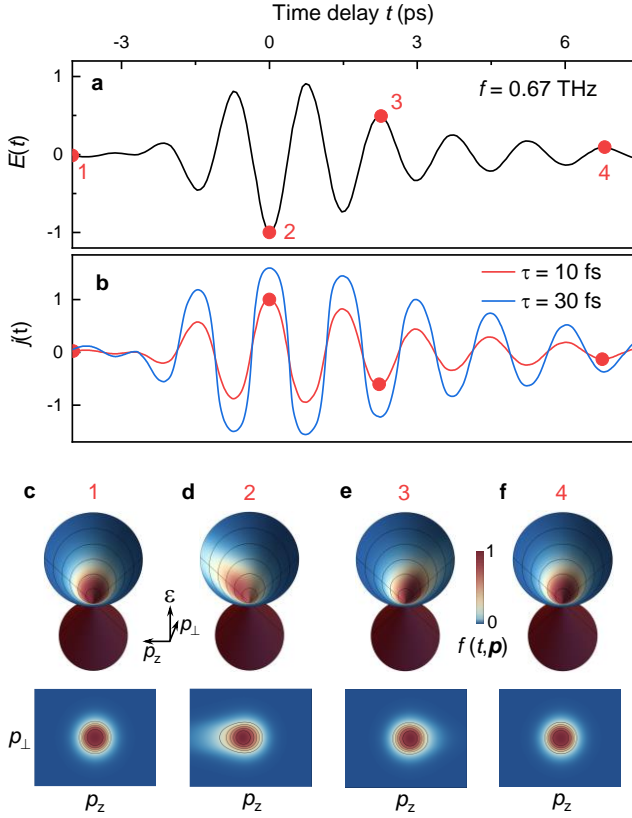


**Fig. 2 | THz-driven nonlinear kinetics and time-resolved distribution function.** **a**, Multicycle pump pulse of  $f = 0.67$  THz characterized in air by its time-dependent electric field  $E(t)$ . **b**, The derived current density  $j(t)$  by solving the Boltzmann equation for  $\tau = 10$  and 30 fs, respectively, for the pump pulse with peak field strength of 110 kV/cm. **c-f**, 3D and 2D illustration of the distribution function  $f(t, \mathbf{p})$  in the upper band of the Dirac cone, corresponding to  $\tau = 10$  fs for various time-delays as marked by the points 1–4 in (a,b), respectively.  $\epsilon$  denotes energy.  $p_z$  denotes momentum component along the linearly-polarized pump-pulse electric field.  $p_\perp$  denotes momentum in the perpendicular direction.

as circularly symmetric in the 2D plots), the obtained strongly stretched and highly asymmetric distribution due to the presence of the strong THz field evidently shows that the electron subsystem is far from thermodynamic equilibrium. As shown in Fig.2f, the electron distribution becomes nearly symmetric in low THz fields, indicating that a quasi-thermalized situation is reconciled in the low-field limit.

For various pump-pulse peak field strength, the intensity of the third-harmonic radiation is shown in Fig.1c for relaxation time  $\tau = 10$  fs. The theoretical results reproduce excellently the observed non-perturbative fluence dependence of the third-harmonic generation up to about 80 kV/cm of the peak field strength, though a deviation from the experimental data occurs at higher fluences. This deviation could be due to enhanced probability of interband multiphoton tunneling in the high electric-field limit, which is not included in our semi-classical analysis. Nevertheless, we found that the non-perturbative dependence on pump-pulse fluence is a generic

feature of the THz driven nonequilibrium states in the Dirac systems. Furthermore, we found that efficiency and fluence-dependence of the THz HHG is very sensitive to the scattering rate  $1/\tau$ . By decreasing the scattering rate (or suppressing the dissipative processes), the transient distribution function is further stretched for the same electric-field strength, resulting in greater current density (c.f.  $\tau = 30$  fs in Fig.2b) and enhanced HHG efficiency.

In order to detect higher-order harmonic radiations, we utilized lower-frequency and strong-field THz pump pulses (see Methods)<sup>42</sup>. Figure 3a shows the observed harmonic radiations up to the seventh order for the pump-pulse frequency of 0.3 THz (see Fig.3b for the waveform). Only the odd-order harmonics are observed, providing the spectroscopic evidence for the existence of inversion symmetry in the crystalline structure of  $\text{Cd}_3\text{As}_2$  (see Ref.<sup>33</sup>). Our experimental results not only set the record for THz HHG in the 3D Dirac materials, but also present the striking observation of the non-perturbative fluence dependence for all the observed harmonic radiations, as presented in Fig.3c-3e.

For the third harmonic radiations, the fluence dependence is also slightly below the cubic power-law dependence, similar to the behavior for the 0.7 THz pump pulse. Moreover, for the higher-order harmonics, the deviation from the corresponding perturbative power-law dependence is further increased. These features are perfectly captured by our quantitative theoretical analysis. By implementing the experimental pump pulse (see Fig.3b) in our calculations, the time-resolved harmonic signals are derived as a function of pump-pulse fluence. The best fitting for all the experimentally observed HHG is achieved at  $\tau = 10$  fs (see Fig.3c-3e). The obtained value of  $\tau = 10$  fs is comparable to that in graphene<sup>43</sup> and while smaller than, is in the same order of magnitude as the estimate from Shubnikov-de Haas measurements<sup>39</sup>. These results strongly indicate that the THz field-driven nonlinear kinetics of the Dirac electrons is the mechanism responsible for the observed non-perturbative nonlinear response in  $\text{Cd}_3\text{As}_2$ . Although for the seventh harmonic the experimental uncertainty is enhanced at the lowest fluence, the fluence dependence far away from the perturbative one is a clear and consistent experimental and theoretical observation. We note that the observed non-perturbative response suggests that the experimental setting is close to but still below the so-called high-harmonic plateau regime, in which the HHG intensity remains almost constant for the high orders and drops abruptly at a cutoff frequency as found in gases as well as in solids<sup>1,14</sup>.

The established mechanism of THz HHG here based on the driven nonlinear kinetics of Dirac electrons is different from those mechanisms proposed for HHG in graphene<sup>11,12,19,24</sup>, in which either the interband transitions were found playing the dominant role or the intraband electron subsystem is

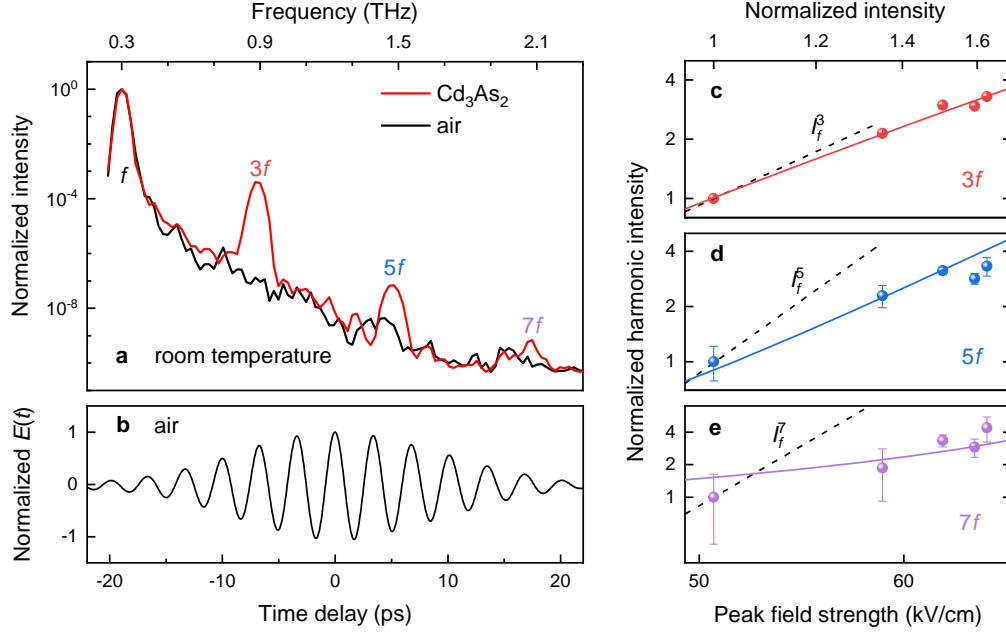


**Fig. 3 | High-harmonic generations in  $\text{Cd}_3\text{As}_2$ .** **a**, Room-temperature spectrum of high-harmonic generations in  $\text{Cd}_3\text{As}_2$  for **b**, multicycle pump pulse of  $f = 0.3$  THz, compared with air as a reference. Pump-intensity dependence of the **c**, third-, **d**, fifth-, and **e**, seventh-harmonic generation (symbols), compared with the perturbative power laws (dashed lines), i.e.  $\propto I_f^3$ ,  $I_f^5$ , and  $I_f^7$ , respectively. In **c,d,e**, the solid lines show the fitted theoretical results corresponding to the relaxation time  $\tau = 10$  fs.

assumed to thermalize quasi-instantaneously. In contrast, in the context of the 3D Dirac system, we found that, firstly, in the presence of strong THz fields, the entire upper-band distribution is strongly stretched and highly asymmetric, denying a description using the Fermi-Dirac distribution of thermodynamic equilibrium states that is symmetric along the Dirac cone. Secondly, for the intraband kinetics, the linear energy-momentum dispersion is crucial for the THz HHG, whereas for a parabolic dispersion the induced radiation field  $E_{out} \propto \frac{dj}{dt} \propto \frac{dv}{dt} \propto E_{in}$  should follow the pump field  $E_{in}$ , hardly yielding harmonics. Thirdly, the exact shape of the electron distribution and its real-time evolution, as obtained from the Boltzmann transport theory, is directly responsible for the THz HHG. A higher efficiency is revealed for the cases of a more strongly stretched and highly asymmetric distribution, due to stronger THz electric field and/or reduced scattering rate.

In conclusion, we have observed THz driven high-harmonic generation up to the seventh order unprecedentedly in the 3D Dirac semimetal  $\text{Cd}_3\text{As}_2$ . The fluence dependence of all the observed HHG was found well beyond the perturbative regime. By performing real-time quantitative analysis of the THz field-driven intraband kinetics of the Dirac electrons using the Boltzmann transport theory, we have established the nonlinear intraband kinetics as the mechanism for the observed THz HHG in  $\text{Cd}_3\text{As}_2$ . The mechanism found here for THz HHG is expected to be universal in the vast family of 3D Dirac and Weyl materials<sup>44</sup>, which provides strategies for pursuing high efficiency of THz HHG, and establishes HHG as a sensitive tool for exploring the interplay of various degrees of

freedom. Towards the higher electric-field regime, an experimental realization of THz HHG plateau in the Dirac materials and a full quantum-mechanical dynamic analysis are still outstanding from both the fundamental and the application points of view.

**Acknowledgements** We acknowledge the ELBE team for operating the ELBE facility, and M. Gensch for support of the experiments. Z.W. thanks A. Renno for characterizing the samples microscopically, and Enke Liu for helpful discussions. S.K. and B.G. acknowledge support from the European Cluster of Advanced Laser Light Sources (EUCALL) project, which has received funding from the European Union's Horizon 2020 research and innovation programme under Grant Agreement No 654220. N.A., S.K., and I.I. acknowledge support from the European Union's Horizon 2020 research and innovation program under grant agreement No. 737038 (TRANSPiRE). R.M.A.D. and P.S. were supported in part by the DFG (German Research Foundation) through the Leibniz Program and ct.qmat (EXC 2147, project-id 39085490). F.X. was supported by National Natural Science Foundation of China (Grant No. 11934005, 61322407, 11474058, 61674040 and 11874116), National Key Research and Development Program of China (Grant No. 2017YFA0303302 and 2018YFA0305601). P.v.L. and Z.W. acknowledge partial support by the DFG via project No. 277146847 - Collaborative Research Center 1238: Control and Dynamics of Quantum Materials (Subproject No. B05).

**Author Contributions** Z.W. and T.O. conceived the project with P.S. S.K. and Z.W. carried out the THz HHG experiments and analyzed the data with S.G., J.-C.D., B.G., I.I., N.A., M.C., M.B. R.M.A.D., P.S. and T.O. performed the theoretical

calculations and analyzed the data. J.L. and F.X. fabricated and characterized the high-quality samples. S.G., P.v.L., and Z.W. characterized linear THz response of the samples. Z.W. wrote

the manuscript with contributions from S.K., R.M.A.D., S.G., J.L., P.S. and T.O. All authors commented the manuscript.

## References

- <sup>1</sup> Corkum, P. B. & Krausz, F. Attosecond science. *Nat. Phys.* **3**, 381 – 387 (2007).
- <sup>2</sup> Drescher, M. *et al.*, X-ray Pulses Approaching the Attosecond Frontier. *Science* **291**, 1923 – 1927 (2001).
- <sup>3</sup> Paul, P. M. *et al.*, Observation of a Train of Attosecond Pulses from High Harmonic Generation. *Science* **292**, 1689 – 1692 (2001).
- <sup>4</sup> Ghimire, S. *et al.*, Observation of high-order harmonic generation in a bulk crystal. *Nat. Phys.* **7**, 138 – 141 (2011).
- <sup>5</sup> Vampa, G. *et al.*, Linking high harmonics from gases and solids. *Nature* **522**, 462 – 464 (2015).
- <sup>6</sup> You, Y. S., Reis, D. A., & Ghimire, S. Anisotropic high-harmonic generation in bulk crystals. *Nat. Phys.* **13**, 345 – 349 (2016).
- <sup>7</sup> Luu, T. T. *et al.*, Extreme ultraviolet high-harmonic spectroscopy of solids. *Nature* **521**, 498 – 502 (2015).
- <sup>8</sup> Schubert, O. *et al.*, Sub-cycle control of terahertz high-harmonic generation by dynamical Bloch oscillations. *Nat. Photonics* **8**, 119 – 123 (2014).
- <sup>9</sup> Hohenleutner, M. *et al.*, Real-time observation of interfering crystal electrons in high-harmonic generation. *Nature* **523**, 572 – 575 (2015).
- <sup>10</sup> Langer, F. *et al.*, Lightwave-driven quasiparticle collisions on a subcycle timescale. *Nature* **533**, 225 – 229 (2016).
- <sup>11</sup> Yoshikawa, N., Tamaya, T., Tanaka, K. High-harmonic generation in graphene enhanced by elliptically polarized light excitation. *Science* **356**, 736 – 738 (2017).
- <sup>12</sup> Bowlan, P. *et al.*, Ultrafast terahertz response of multilayer graphene in the nonperturbative regime. *Phys. Rev. B* **89**, 041408 (2014).
- <sup>13</sup> Giorgianni, F. *et al.*, Strong nonlinear terahertz response induced by Dirac surface states in Bi<sub>2</sub>Se<sub>3</sub> topological insulator. *Nat. Commun.* **7**, 11421 (2016).
- <sup>14</sup> Ghimire, S. & Reis, D. A. High-harmonic generation from solids. *Nat. Phys.* **15**, 10 – 16 (2019).
- <sup>15</sup> Matsunaga, R. *et al.*, Light-induced collective pseudospin precession resonating with Higgs mode in a superconductor. *Science* **345**, 1145–1149 (2014).
- <sup>16</sup> Rajasekaran, S. *et al.*, Probing optically silent superfluid stripes in cuprates. *Science* **359**, 575 – 579 (2018).
- <sup>17</sup> Chu, H. *et al.*, New collective mode in superconducting cuprates uncovered by Higgs spectroscopy. Preprint, arXiv:1901.06675 (2019).
- <sup>18</sup> Yang, X. *et al.*, Lightwave-driven gapless superconductivity and forbidden quantum beats by terahertz symmetry breaking. *Nat. Photonics* **13**, 707 – 713 (2019).
- <sup>19</sup> Hafez, H. A. *et al.*, Extremely efficient terahertz high-harmonic generation in graphene by hot Dirac fermions. *Nature* **561**, 507 – 511 (2018).
- <sup>20</sup> Huttner, U., Kira, M. & Koch, S. W. Ultrahigh Off-Resonant Field Effects in Semiconductors. *Laser Photon Rev.* **11**, 1700049 (2017).
- <sup>21</sup> Silva, R. E. F. *et al.*, High-harmonic spectroscopy of ultrafast many-body dynamics in strongly correlated systems. *Nat. Photonics* **12**, 266 – 270 (2018).
- <sup>22</sup> Vampa, G. *et al.*, Theoretical Analysis of High-Harmonic Generation in Solids. *Phys. Rev. Lett.* **113**, 073901 (2014).
- <sup>23</sup> Kemper, A. F. *et al.*, Theoretical description of high-order harmonic generation in solids. *New J. Phys.* **15**, 023003 (2013).
- <sup>24</sup> Soavi, G. *et al.*, Broadband, electrically tunable third-harmonic generation in graphene. *Nat. Nanotechnol.* **13**, 583 – 588 (2018).
- <sup>25</sup> Mikhailov, S. A. & Ziegler, K. Nonlinear electromagnetic response of graphene: frequency multiplication and the self-consistent-field effects. *J. Phys.: Condens. Matter* **20**, 38420 (2008).
- <sup>26</sup> Ishikawa, K. L. Nonlinear optical response of graphene in time domain. *Phys. Rev. B* **82**, 201402 (2010).
- <sup>27</sup> Al-Naib, I., Poschmann, M., & Dignam, M. M. Optimizing third-harmonic generation at terahertz frequencies in graphene. *Phys. Rev. B* **91**, 205407 (2015).
- <sup>28</sup> Wang, Z. *et al.*, Three-dimensional Dirac semimetal and quantum transport in Cd<sub>3</sub>As<sub>2</sub>. *Phys. Rev. B* **88**, 125427 (2013).
- <sup>29</sup> Ali, M. N. *et al.*, The Crystal and Electronic Structures of Cd<sub>3</sub>As<sub>2</sub>, the Three-Dimensional Electronic Analogue of Graphene. *Inorg. Chem.* **53**, 4062 – 4067 (2014).
- <sup>30</sup> Liu, Z. K. *et al.*, A stable three-dimensional topological Dirac semimetal Cd<sub>3</sub>As<sub>2</sub>. *Nat. Mater.* **13**, 677 – 681 (2014).
- <sup>31</sup> Borisenko, S. *et al.*, Experimental Realization of a Three-Dimensional Dirac Semimetal. *Phys. Rev. Lett.* **113**, 027603 (2014).
- <sup>32</sup> Neupane, M. *et al.*, Observation of a three-dimensional topological Dirac semimetal phase in high-mobility Cd<sub>3</sub>As<sub>2</sub>. *Nat. Commun.* **5**, 3786 (2014).
- <sup>33</sup> Crassee, I. *et al.*, 3D Dirac semimetal Cd<sub>3</sub>As<sub>2</sub>: A review of material properties. *Phys. Rev. Mater.* **2**, 120302 (2018).
- <sup>34</sup> Zhang, C. *et al.*, Evolution of Weyl-orbit and quantum Hall effect in Dirac semimetal Cd<sub>3</sub>As<sub>2</sub>. *Nat. Commun.* **8**, 1272 (2017).
- <sup>35</sup> Zhang, C. *et al.*, Quantum Hall effect based on Weyl orbits in Cd<sub>3</sub>As<sub>2</sub>. *Nature* **565**, 331–336 (2018).
- <sup>36</sup> Uchida, M. *et al.*, Quantum Hall states observed in thin films of Dirac semimetal Cd<sub>3</sub>As<sub>2</sub>. *Nat. Commun.* **8**, 2274 (2018).
- <sup>37</sup> Schumann, T. *et al.*, Observation of the Quantum Hall Effect in Confined Films of the Three-Dimensional Dirac Semimetal Cd<sub>3</sub>As<sub>2</sub>. *Phys. Rev. Lett.* **120**, 016801 (2018).
- <sup>38</sup> Moll, P. J. W. *et al.*, Transport evidence for Fermi-arc-mediated chirality transfer in the Dirac semimetal Cd<sub>3</sub>As<sub>2</sub>. *Nature* **535**, 266 – 270 (2016).
- <sup>39</sup> Liu, Y. *et al.*, Gate-tunable quantum oscillations in ambipolar Cd<sub>3</sub>As<sub>2</sub> thin films. *NPG Asia Mater.* **7**, e221 (2015).
- <sup>40</sup> Bhatnagar, P. L., Gross, E. P., & Krook, M. A Model for Collision Processes in Gases. I. Small Amplitude Processes in Charged and Neutral One-Component Systems. *Phys. Rev.* **94**, 511 (1954).
- <sup>41</sup> Xiao, D., Chang, M.-C., & Niu, Q. Berry phase effects on electronic properties. *Rev. Mod. Phys.* **82**, 1959 (2010).
- <sup>42</sup> Green, B. *et al.*, High-field high-repetition-rate sources for the coherent THz control of matter. *Sci. Rep.* **6**, 22256 (2016).
- <sup>43</sup> Gierz, I. *et al.*, Snapshots of non-equilibrium Dirac carrier distributions in graphene. *Nat. Mater.* **12**, 1119 – 1124 (2013).
- <sup>44</sup> Armitage, N. P., Mele, E. J., & Vishwanath, A. Weyl and Dirac semimetals in three-dimensional solids. *Rev. Mod. Phys.* **90**, 015001 (2018).